

Safe Distance Detection Method of Unmanned Vehicle Based on Virtual Reality

Lingfang Wu*

College of Automobile and Transportation Engineering, Guilin University of Aerospace Technology, Guilin 541004, China

Unmanned vehicles can enter and leave dangerous airspace for a long time and play a vital role in critical missions. They carry special equipment to accomplish specific tasks with high cost. They have great application prospects and strategic value, so it is essential to study their operational safety. This paper proposes a safe distance detection method based on virtual reality technology for driverless cars, and simulates the special effects of 3D graphics of driverless cars, 3D graphics of terrain and geomorphology, sound, and smoke from explosion by using virtual reality technology. Threshold segmentation and refinement methods are used to reduce the computation of obstacle recognition in the constructed virtual reality scene, and the decision tree recognition method is used to identify obstacles. The location of obstacles is determined, and then the three-dimensional Euler space image is transformed into a two-dimensional Euler space image by constructing the ranging model. The detection of the safe distance of unmanned vehicles is achieved by using the monocular camera ranging model. The experimental results show that the detection method can clearly and effectively simulate a road environment and an explosion site environment, and can accurately and efficiently detect the safe distance of the unmanned vehicle in the conventional environment and in a complex electromagnetic environment, so as to enhance the safety of the unmanned vehicle.

Keywords: Virtual reality, Unmanned vehicle, Operation, Safety distance, Detection, Obstacles

1. INTRODUCTION

With the development of society and the progress of science and technology, ‘robots’ are being used more and more in various contexts: military, scientific research, manufacturing and daily life. Unmanned vehicles, also known as autonomous vehicles, intelligent vehicles, outdoor wheeled mobile robots and so on, involve cognitive science, artificial intelligence, robotics and vehicle engineering and other interdisciplinary disciplines. They are comprehensive test beds and ideal carriers of various emerging technologies. They are also an important development direction of current cutting-edge science and technology (Sang et al. 2016). At the same time, an unmanned aerial vehicle is small, simply-structured, lightweight, easy to use and maintain, and has good flexibility (Dahmani et al., 2015); hence, it has great development

potential and good application prospects. Because it is unmanned, it can enter and exit dangerous airspace for a long time, often playing a critical role. The research on unmanned vehicles involves not only breakthroughs in theoretical methods and key technologies, but also a large number of engineering and experimental problems. Its significance is reflected not only in the core scientific issues involved, but also in its great application prospects and strategic value; hence, this particular technology is attracting much attention not only from researchers and developers, but also from the general public.

Specifically, whether in daily life or in military and scientific research, the purpose of having unmanned vehicles is to completely or partially replace the functions of drivers, and the key technologies involved are the same. In daily life, the driving of vehicles can be not only boring but also dangerous. Drivers need to always pay attention to changes in the environment. At the same time, they need to overcome

*Email of corresponding author wulfguat@163.com

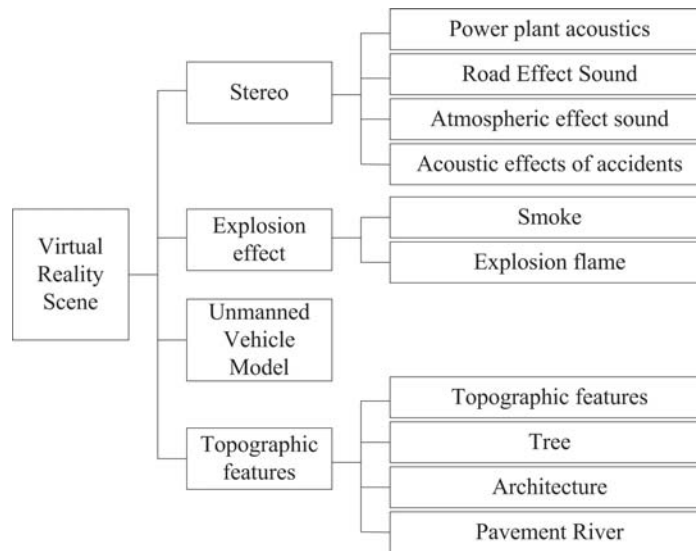


Figure 1 Model Tree Relations of Different Sceneries.

physical and potentially dangerous issues such as fatigue and carelessness. Unmanned driving and its derivative technology can free drivers from tedious driving behavior to a certain extent. In the military sphere, unmanned driving technology can replace human beings, carrying out dangerous missions such as reconnaissance, mine clearance, radiation and battle field hazards, so as to reduce casualties (Wu et al., 2017). In scientific research, unmanned vehicles can help humans to engage in extra terrestrial activities such as the exploration of the moon and Mars (Minaeian et al., 2017).

Since 2000, with the rapid development of virtual reality technology, computer vision, artificial intelligence, electronic circuits and other disciplines, these and other technologies have also been widely used in vehicles. In recent years, researchers have begun to focus on assisted driving technology. Autonomous parking, adaptive cruise, dangerous overtaking alarm, lane departure alarm and other functions have been widely used in unmanned vehicles.

In spite of this, there are still many problems to overcome before fully realizing unmanned driving in complex traffic environments. The urban road environment is large, complex and changeable; in rural road environments, roads twist and turn, and road conditions are not good; in highway environments, vehicle speed is faster, with high risk (Xu & Barbic, 2017). Moreover, the control of unmanned vehicles is a relatively complex process, requiring a relatively high level of operator. In addition to the knowledge of aerodynamics and atmospheric turbulence, it also requires the operator to be familiar with the aerodynamic characteristics of this type of unmanned vehicle, with certain control experience and good psychological quality. An unmanned vehicle may be carrying special equipment to accomplish specific tasks, and the cost is high. Therefore, its operational safety is most important. Therefore, it is essential to have a safe distance detection method for unmanned vehicles. In this paper, a method based on virtual reality is proposed to detect the safe distance of unmanned vehicles. Utilizing virtual reality technology, various scenarios are constructed, road obstacles are detected, and the safe distance of unmanned

vehicles is detected by means of a distance measurement model.

2. MATERIALS AND METHODS

2.1 Realization of Virtual Reality Scene Simulation

A virtual reality scene is comprised of various elements, and the corresponding virtual simulation environment is simulated by different kinds of models. The simulation processing for three-dimensional virtual reality of different kinds of sceneries is different, and there are also various challenges that must be overcome in terms of concrete implementation. Various scene models are divided into the following parts according to different processing methods or modeling and simulation methods:

- (1) Modeling and processing of unmanned vehicle model
- (2) Processing and modeling of large terrain
- (3) Processing of surface buildings and trees
- (4) Audio simulation
- (5) Three-dimensional simulation of special effects such as flame and smoke following an explosion

2.1.1 Data Organization and Processing of the Whole Scene

The creation of a scene requires a great deal of data. According to the relationship among various scenery elements in the scene, the model data are organized and processed according to the tree structure (Lee et al., 2015). The model tree relationship of various scenes is shown in Fig. 1, in which the child nodes of each node have relatively independent operation processing, and their joint processing is determined by their father nodes (Parijat et al., 2015).

2.1.2 3-D Graphic Simulation of Unmanned Vehicle

The simulation graphics model of the unmanned vehicle can be created in two ways: modeling in programming and importing models in programming using modeling software (Aravind et al., 2015). Because it is very difficult to build models in programming, it is much easier to use 3D MAX and other modeling software to build models, making it easier to obtain realistic models. Therefore, the 3-D graphics simulation of unmanned vehicles is modeled using 3D MAX software, and the interface provided by WTK is used to import the models directly in the program. Initialization requires that the unmanned vehicle be at the center of the scene, and the coordinate system of the body of the unmanned vehicle coincides with the coordinate system of the simulation scene, which is called the 'initial standard attitude' (Zhong et al., 2015). However, the pose of the imported model does not generally meet this requirement, so the model needs to be corrected to some extent. Manual calibration is cumbersome and inconsistent; thus, it needs to be automatically calibrated by the program.

(1) Attitude calibration of unmanned vehicle model

Any attitude of the model can be regarded as a standard position model, which rotates a certain angle α , β , and γ around three axes (x , y , z) of the coordinate system, and then translates a certain displacement. Then the displacement vector of the model can be obtained by the center position (x_c, y_c, z_c) of the model, and then the model can be moved—(x_c, y_c, z_c) to get another model position coinciding with the center of the standard position, which is the current position. There is the following relationship between the model coordinate (x_m, y_m, z_m) of the standard position and the corresponding point coordinate (x'_m, y'_m, z'_m) of the current position:

$$\begin{bmatrix} x'_m \\ y'_m \\ z'_m \end{bmatrix} = \begin{bmatrix} 1 & 0 & 0 \\ 0 & \cos \alpha & -\sin \alpha \\ 0 & \sin \alpha & \cos \alpha \end{bmatrix} \begin{bmatrix} \cos \beta & 0 & -\sin \beta \\ 0 & 1 & 0 \\ \sin \beta & 0 & \cos \beta \end{bmatrix} \times \begin{bmatrix} \cos \gamma & -\sin \gamma & 0 \\ \sin \gamma & \cos \gamma & 0 \\ 0 & 0 & 1 \end{bmatrix} \quad (1)$$

When the standard position of the unmanned vehicle is in the center, the longitudinal axis coincides with the z axis, the head is in the positive direction of the z axis, and the symmetrical plane is yoz plane, the center point a of the head is on the z axis, and the coordinate of the point is $\begin{bmatrix} 0 \\ 0 \\ z_a \end{bmatrix}$.

Formula (1) is substituted to obtain the relationship between the coordinate of point a of the unmanned vehicle's current position and the coordinate of point a of the standard position is as follows:

$$\begin{bmatrix} x'_a \\ y'_a \\ z'_a \end{bmatrix} = \begin{bmatrix} z_a \bullet \cos \beta \\ z_a \bullet \sin \alpha \bullet \sin \beta \\ -z_a \bullet \cos \alpha \sin \beta \end{bmatrix} \quad (2)$$

It can be seen from Formula (2), $\beta = \arccos\left(\frac{x'_a}{z_a}\right)$ and then Formula (2) is substituted to obtain $\alpha = \arctg\left(\frac{y'_a}{z'_a}\right)$.

When the model is in the standard position, the coordinate of point b at the center of the tail should be $\begin{bmatrix} 0 \\ y_b \\ z_b \end{bmatrix}$. The coordinate of point b correspond to the current position is $\begin{bmatrix} x'_b \\ y'_b \\ z'_b \end{bmatrix}$.

Substitution of Formula (1) can be solved as:

$$\gamma = \arccos\left[\frac{y'_b \cos \alpha + z'_b \sin \alpha}{y_b}\right] \quad (3)$$

The model can be automatically calibrated to the standard attitude by the values of α , β and γ (Ns et al., 2016). That is to say, firstly the model is moved to the center and coincides with the original point, and then it is rotated around the x , y and z axes in turn $-\alpha$, $-\beta$, $-\gamma$, which becomes the standard attitude.

(2) Motion simulation of unmanned vehicle model

In the simulation process, the attitude of the unmanned vehicle model is changed according to the vehicle pose obtained from the mathematical simulation module (Hu et al., 2018). The main parameters of position and attitude are the position of the unmanned vehicle in the ground coordinate system and the three Euler angles of the unmanned vehicle. When the real-time motion attitude is obtained from the standard position of the vehicle, the corresponding angles are rotated around z , x and y axes respectively according to the rolling angle, pitch angle and yaw angle of the unmanned vehicle.

2.1.3 3D Graphic Simulation of Topography and Landform

(1) Simulation of large-scale terrain

An unmanned vehicle has a wide range of flight activities. The simulation of an unmanned vehicle must achieve large-scale terrain simulation. The digital elevation data of the terrain are used to construct a real-time 3-D graphical simulation model of terrain (Zhang et al., 2018). According to the position of the current view point, the corresponding terrain data are read, and then the grid model of the terrain model is constructed in real time. Because of the low image processing ability of PC, the number of patches in the scene must be reduced as much as possible, so an optimization algorithm is adopted for the terrain model. The merging of simultaneous flight patches is preferred. The elevation data can be read while the grid is being established (i.e. simultaneously) and the terrain grid can be established while the optimization is being completed.

(2) Simulation of surface buildings and trees

Various methods are used to simulate buildings, roads, rivers, bridges and trees. Buildings are combinations of simple geometries, which are simulated by means of real three-dimensional models. The visual effects of roads and rivers need only one plane, so there is no need to build three-dimensional models. The models of roads and rivers are two-dimensional and their surfaces are constructed using appropriate textures and materials to achieve simulation

(Ziraknejad et al., 2015). There are too many three-dimensional models of trees to achieve the goal of real-time simulation on a PC. Billboard technology is also very realistic, although not as much as the three-dimensional model. In the scene, a billboard patch is used to simulate a tree. The pseudocode for drawing trees is:

```

Read the tree's position in the scene (x, y, z);

Calculate the z value of the coordinates of each tree
relative to the viewpoint.

The trees are sorted from small to large according to z
value.

For each sorted tree, it is drawn in turn.
    Set up the rendering mode and turn on the depth
    detection.

The source factor of the facility fusion mode is the source
alpha value, and the target factor is (source alpha value).

    Rotate the current coordinate system to the view-
    point direction.

    Move the coordinate system to the pilot position of
    the tree.

    Rotate the current coordinate system to the scene
    coordinate direction.

The current coordinate around the Z axis to rotate the
viewpoint.

Draw trees with corresponding texture.

Rotate the current coordinates and rotate the each odd
number of the rotation of the viewpoint around the Z
axis.

Rotate the current coordinate system in the opposite
direction to the viewpoint.

    Move the coordinate system to the pilot position of
    the tree.

    Rotate the current coordinate system to the scene
    coordinate direction;

Draw the next tree in a loop.

```

2.1.4 Audio Simulation

Realistic sound effects not only make the operator feel immersed in the scene, but also help the operator to judge the state of the vehicle. The main sounds to be simulated are those of the power plant, the road, the immediate environment and the accident (Gke et al., 2015).

Directx is used to program and simulate the sound. Directx provides a wealth of functions, which can directly set the location of the sound source and listener in the three-dimensional environment, and calculate the output from the low-level function to achieve the simulation effect of a three-dimensional stereo. Four different sound sources are set for four different sound effects in the scene. According to the

position of the viewpoint and the position of the unmanned vehicle in the scene, the position of the relevant sound sources and the position of the listener can be set synchronously to achieve a realistic three-dimensional sound effect.

2.1.5 3-D Simulation of Special Effects Such as Explosion Flame Smoke

Special effects of accidents caused by vehicles include explosions, flames and smoke. Outdoor environment also often has the effect of fog, rain and snow. Billboard technology is used to simulate explosion and flame. Unlike tree simulation, the texture on the face of explosion flame is dynamic, and different textures of the dynamic process of explosion and flame are pasted with time. The simulation of smoke is based on the particle system, because it only needs hundreds of facets in order to obtain realistic smoke. The fog simulation uses the functions provided by the software platform to directly achieve the fog effect. The simulation of rain and snow uses a facet close to the viewpoint, whose size covers the whole screen and circularly pastes the texture of the dynamic process of rain and snow.

2.2 Detection of Road Obstacles

The process of road obstacle detection is the process of identifying and calibrating the target object in the virtual reality scene (Wan et al., 2017). Firstly, the pretreated virtual reality scene is processed by the threshold segmentation and refining methods to reduce the computational load, and then obstacles in the virtual reality scene are identified.

2.2.1 Segmentation of Road areas

According to some characteristics of the elements in the scene, the real image is divided into several regions, so that the performance characteristics of different regions are distinctly different. Threshold segmentation is fast and stable, and can play a better role in a specific environment (Peng et al., 2015). Specific algorithms are applied: (1) to determine the location of segmentation; (2) to compare and classify the segmentation threshold and the pixel value. The image is extracted from the bottom of the virtual reality image and the gray histogram is counted. According to the histogram, the gray statistical information of the road is obtained. Then the basic position of the road is judged by the gray information (Wu et al., 2016). The basic process of obtaining the threshold and detecting the road area is as follows:

- Step 1: Select the area below the road to determine whether the area contains two kinds of gray values: road surface and marking. If no marking is included, step 3 is executed next.
- Step 2: Select the initial threshold T_0 , and use the iteration method to get the segmentation threshold of two kinds of gray levels. Use the threshold to exclude the influence of the marking line, and obtain the independent gray level of the road.

Step 3: The upper and lower limits $_u$ and $_d$ of gray level in the road area are calculated by using p — parameter method.

Step 4: Use $_u$ and $_d$ to divide the road area in the virtual reality image.

2.2.2 Binary Image Refining

After image segmentation according to the acquired threshold, the basic area of the lane is obtained. In order to reduce the computational complexity of obstacle detection, image refining is needed.

Refining is the operation of reducing the line width of the binary image to one pixel. The line obtained after refining is called the ‘core line’ (Guo et al., 2016). In the refining process, the core line width is changed to one pixel; the core line position is placed in the center of the original line width; the continuity of the graphics is maintained; and processing is terminated if it is taking too long.

The mathematical morphological refinement method is defined as:

$$S \otimes B = S / S * B \quad (4)$$

In Formula (4): B is a structural element and $S * B$ is a thinning algorithm. It relies on the hit-miss transformation of mathematical morphological image processing. The transformation requires two structural elements E and F . These two structural elements are combined into a structural element pair $B = (E, F)$ to detect the interior and exterior of the image, which is defined as:

$$A * B = (A \ominus E) \cap (A^C \ominus F) \quad (5)$$

Formula (5), A is the original image. It shows that the points in the result set should satisfy two conditions at the same time, and the representational point of the composite structural element E in x should be included in A , and F in A^C .

2.2.3 Recognition of Road Obstacles

The result of obstacle recognition is only “yes” or “no”. Therefore, the decision tree recognition method in syntactic pattern recognition is used to classify the obstacle patterns by a series of sentences and make visual judgments (Wei et al., 2017). It does not involve the problems of spatial transformation and measurement. At the same time, the method can be easily expressed by computer judgement statements and is easy to implement.

According to certain discriminant conditions, the location of obstacles can be obtained by eliminating pedestrians and non-motor vehicles in the image using a decision tree. In the process of recognition, a decision tree is established according to the relevant factors: (1) in the road area; (2) the gray level of the target connected area is different from that of the road area; (3) the basic shape and scope of the connected area. The decision tree method is fast in terms of calculation and can make full use of prior knowledge. When the specific position of obstacles in the image is obtained, the location of obstacles in real space can be further calculated according to the image

position, and then the safe distance between the unmanned vehicle and the obstacle can be obtained through the ranging model.

2.3 Establishment of Ranging Model

To complete the calculation of the safe running distance of an unmanned vehicle, a distance measurement model should be established. The process of capturing a virtual reality image by camera is an image transformation process from three-dimensional Eulerian space to two-dimensional Eulerian space (Wang et al., 2016). The measurement of data in real space from image data can be regarded as the inverse of the above process in a sense. The construction of the model is based on the theory of image transformation.

2.3.1 Image Transformation Theory

Geometric transformation is a mapping function between an image and all points in its deformed image (Wang 2015). It can be expressed as:

$$[x, y] = [X(u, v), Y(u, v)] \text{ or } [u, v] = [U(x, y), V(x, y)] \quad (6)$$

In formula (6), $[x, y]$ is the coordinate of the input image pixel, $[u, v]$ is the coordinate of the output image pixel, and X, Y, U and V are the mapping functions that uniquely determine the spatial transformation; that is, they uniquely define the geometric correspondence between the input image and all points in the output image. X and Y map input to output, which is called forward mapping; U and V map output to input, which is called reverse mapping.

Spatial transformations are usually represented by transformation matrices, such as:

$$[x', y', w'] [u, v, w]^T \quad (7)$$

In Formula (7), x' and y' are the expressions of x and y ; w' and w are the homogeneous coordinates introduced by the homogeneous processing of future and three-dimensional matrices.

Camera acquisition of virtual reality images involves image coordinate system, camera coordinate system and world coordinate system. In Fig. 2, the image coordinates X_c and Y_c are defined on the image. The coordinates of each pixel are the number of rows and columns of the pixel in the array. The Z axis of the camera coordinate system is perpendicular to the image plane, and the $X Y$ plane is parallel to the image plane. Since the camera can be placed in any position, it is necessary to select a reference coordinate system to describe the position of the camera and use it to describe the position of any object. The coordinate system is called the world coordinate system and is represented by x, y, z . The image plane is reversed relative to the focus to avoid using a mirror image with negative coordinates.

2.3.2 Establishment of Ranging Model for Monocular Camera

Considering the geometric transformation process of monocular camera ranging, if I is used to represent three-dimensional

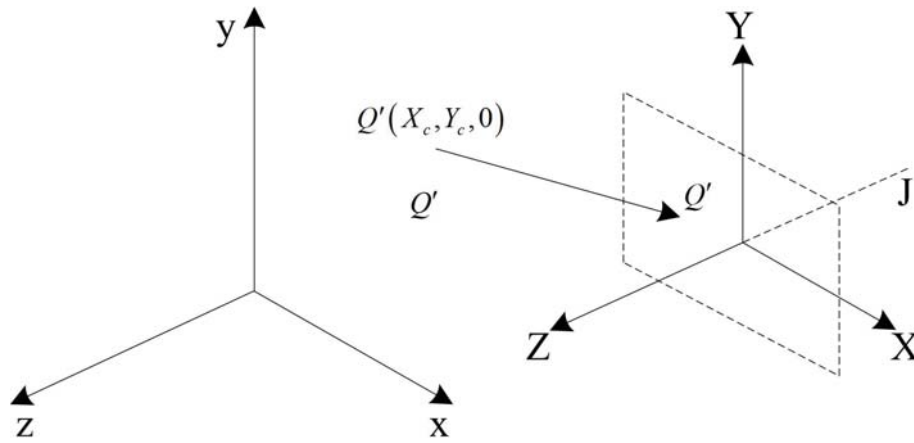


Figure 2 Image Coordinate System, Camera Coordinate System and World Coordinate System.

real space and w is used to represent image space, the image acquisition process is from I to w (Liu et al., 2017). If the origin of the world coordinate system is on the ideal ground ahead, the process of safe distance detection can be regarded as the process of calculating the data on a plane $S = \{(x, 0, z)\}$ in the world coordinate system $I = \{x, y, z\}$ under certain prior conditions using the data in the image space $w = \{X_c, Y_c\}$.

After obtaining the ordinate Y_c of the bottom of the target vehicle in the image space, it is necessary to obtain the conditions of image acquisition and the hypothesis of image scene description. The position of the camera is represented by its position l , d and h in the world coordinate system; the view direction is represented by the angle V^- and θ^- between the central axis of the camera and the standard axis; the aperture angle of the camera is $2T$; and the camera clarity is $n \times n$. The above parameters can be obtained by measurement or calculation. From the camera to the outside space, $n \times n$ ray obtains the angle value of the ray of point (X_c, Y_c) of the image space in the actual space, which is determined by θ and V .

$$\theta = (\theta^- - T) + Y_c \frac{2T}{n-1} \quad (8)$$

In Formula (8), Y_c is the coordinate in image space, $Y_c = 0, 1, \dots, n-1$. In addition, the ground distance d_p from a point p on the ground to the camera in the plane S can be obtained by formula (9):

$$d_p = \frac{h}{\tan \theta}. \quad (9)$$

Based on the above factors, the formula for calculating the safe distance of unmanned vehicles is obtained as:

$$d_p = \frac{h}{\tan \left[(\theta^- - T) + (Y_c) \frac{2T}{n-1} \right]} \quad (10)$$

The model establishes the data relationship between coordinate value Y_c in image space and plane S in real space by using the relation of ray angle. Therefore, the actual position of the vehicle in the plane S can be calculated by obtaining the pixel coordinates of the vehicle in the virtual reality scene image. If the central axis of the camera is parallel to the z axis in the world coordinate system, the values of V^- and θ^- are both 0. The calculation process can also be simplified as:

$$d_p = \frac{h}{\tan \left[\frac{2TY_c}{n-1} - T \right]} \quad (11)$$

3. RESULTS

3.1 Simulation Results of Virtual Reality Field

The experiment takes a certain type of unmanned vehicle as the experimental object, and uses the proposed method based on virtual reality to carry out virtual scene simulation. The results are shown in Fig. 3.

Analysis of Fig. 3 shows that the proposed method can clearly and effectively simulate a road environment and explosion accident environment, which shows that the virtual reality simulation performance of this method is better.

3.2 Experimental Results of Detection Performance in Conventional Environment

On the basis of computer ranging program, the detection of a safe driving distance for an unmanned vehicle captures the image of the vehicle in front of it through virtual reality technology. The calculation value of the driving safe distance of unmanned vehicle is obtained through ranging program processing. The calculation value obtained in a conventional environment is compared with the actual safe distance, and the detection method in this paper is evaluated. The straight road section is selected for the experiment, and the relevant experimental parameters are shown in Table 1.

Five different distances are selected to test the safe distance of the unmanned vehicle. The test results are compared with the actual distance. The test data, error and processing time are shown in Table 2.

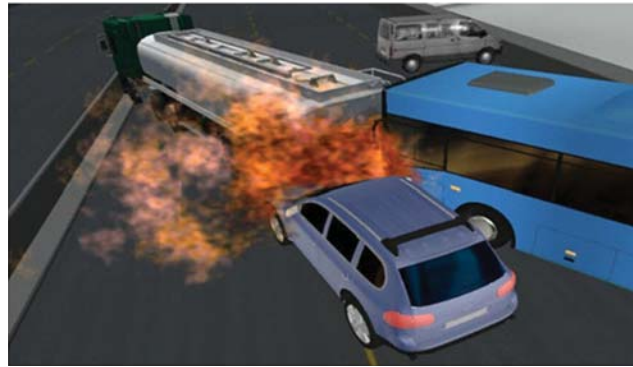
In Table 2, by comparing the running safe distance obtained from the detection experiment and the actual safe distance of the unmanned vehicle, it is proved that the detection method proposed in this paper can detect obstacles and calculate more



(a) Virtual Reality Scene 1 - Road



(b) Virtual Reality Scene 2-Road



(c) Virtual Reality Scene 3 - Explosion

Figure 3 Virtual Reality Field Simulation.

Table 1 Basic Parameters of Safe Distance Detection Experiment.

Parameter name	Parameter values
V^-	0
θ^-	0
Aperture Angle of Camera ($2T/^\circ$)	0.3236
Camera clarity ($n \times n$)	2048×1536
Distance between Camera and Ground (h/m)	1.11

Table 2 Test Data of Safe Distance Detection for Unmanned Vehicles.

Serial number	1	2	3	4	5
Actual distance/m	20	40	60	80	100
Detection result/m	20.45	40.78	64.95	86.26	92.31
Error/m	0.45	0.78	4.95	6.26	7.39
Relative error/%	2.25	1.95	8.25	7.81	7.39
Processing time/100 ms	4	4	3	3	4

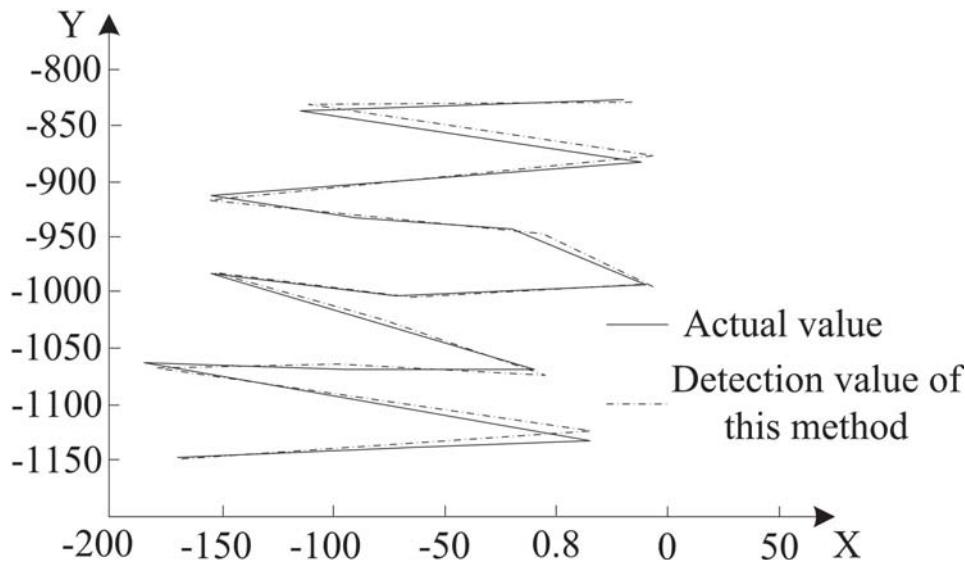


Figure 4 Safe Distance Detection Results of Ranging Model.

accurately the distance between the unmanned vehicle and the obstacle. The image processing and calculation time is less than 1 s. The experimental results show that this method can accurately and efficiently detect the safe distance of unmanned vehicles.

3.3 Experimental Results of Precision Measurement Under Complex Electromagnetic Environment

Experiments are carried out to determine the performance of the proposed detection method. In the complex electromagnetic environment, the safe distance detection experiment is carried out by using the unmanned vehicle ranging model. The safe distance obtained by the ranging model is compared with the actual safe distance, and the results are shown in Fig. 4.

Analysis of Fig. 4 shows that the result of the safe distance detected by the ranging model in this paper overlaps about 40% of the actual safe distance, and the deviation of the remaining 60% is also small. The experimental results show that the proposed ranging model can detect long-distance safe distance of unmanned vehicles in complex electromagnetic environment, and can improve the obstacle-avoidance performance of unmanned vehicles.

3.4 Detection Results of Moving Targets

In order to verify the detection performance of the moving target detection method, several different moving targets are set up. The proposed method is used to detect moving targets. 2# moving target is taken to represent simple shape and 4# moving target is used to represent complex shapes as examples, the detection results and actual results of the two moving targets are compared as shown in Table 3.

Table 3 shows that the velocity magnitude error and velocity direction error are 11.20% and 6°, respectively, when detecting the simple shape of the moving object numbered

2#. When detecting the moving object numbered 4# with complex shape, the velocity magnitude error and velocity direction error are increased by 2.20% and 2°, respectively. The experimental results show that the detection performance of the proposed method is better than that of the moving object with a complex shape.

3.5 Comparisons of Obstacle Target Detection Efficiency

Experiments compare the time-consuming of the proposed detection method, PSD-based method and CAN-bus-based method, in the process of obstacle tracking and detection. The results are shown in Fig. 5.

From Fig. 5, it can be seen that the time-consumption of each frame in tracking and detecting obstacles with the proposed detection method is basically kept within 150 000 us, while the time-consumption of the other two methods is controlled within 175 000 us and 180 000 us, which are higher than that of the proposed method. The experimental results show that the proposed detection method has high real-time performance in tracking and detecting obstacles and can maximize the improvement of unmanned vehicles' operational safety.

3.6 Comparison of Stability in Complex Electromagnetic Environment

In order to test the stability of the proposed detection method in the complex electromagnetic environment, the average interruption probability of three different detection methods is compared in the laboratory. The results are depicted in Fig. 6.

Analysis of Fig. 6 shows that when the average signal-to-noise ratio of the electromagnetic environment near an unmanned vehicle does not exceed 18 dB, the average interruption probability of the detection method proposed in this paper is smaller than that of the other two detection

Table 3 Moving Target State Detection.

Obstacle Number	2#	4#
Actual velocity	25.0	35.0
Actual velocity direction	355°	175°
Detection speed	22.2	30.3
Detection of velocity direction	1°	183°
Speed magnitude error	11.20%	13.40%
Velocity direction error	6°	8°

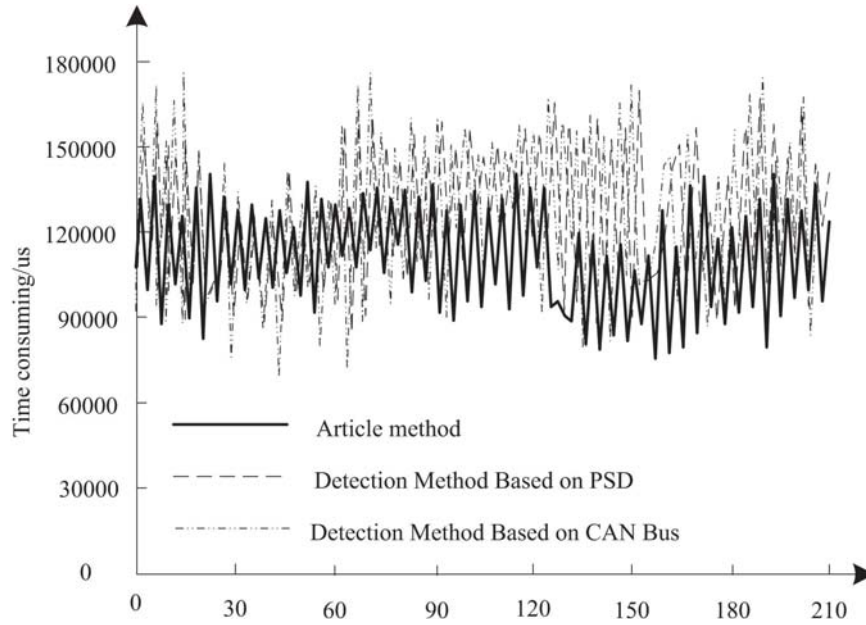


Figure 5 Time-Consuming Situation in Obstacle Tracking and Detection With Different Detection Methods.

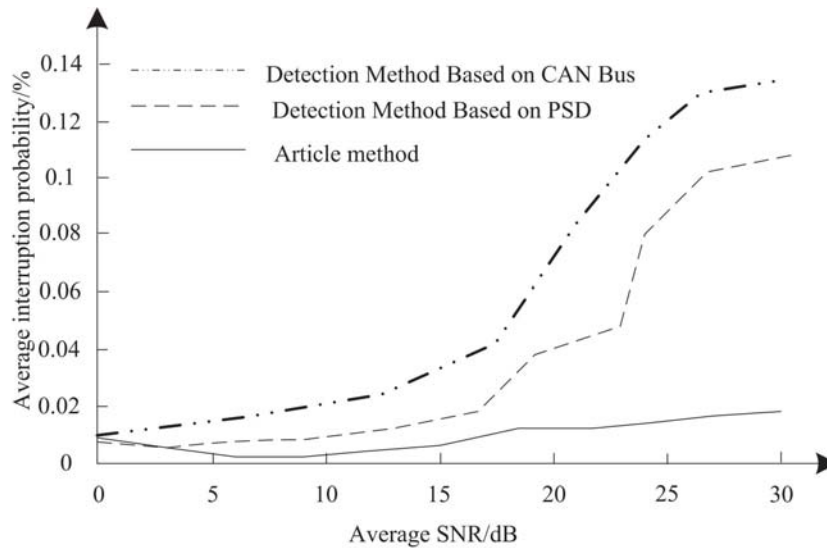


Figure 6 Average Interruption Probability of Different Detection Methods in Complex Electromagnetic Environment.

methods; when the average signal-to-noise ratio of the electromagnetic environment near an unmanned vehicle exceeds 18 dB, the interruption probability of the three different detection methods increases with the average signal-to-noise ratio. The average interruption probability growth

curve of the detection method in this paper is the gentlest, far less than the average interruption probability of the other two detection methods, which shows that the detection method in this paper has better stability in a complex electromagnetic environment.

4. DISCUSSION

In the last section, the experiments validate the performance of the proposed detection method. The experiments show that this detection method can clearly and effectively simulate the road environment and explosion accident environment, accurately detect the safe clustering of unmanned vehicles in both a conventional environment and a complex electromagnetic environment, and can detect the speed error of simple-shape moving targets. Compared with the other two detection methods, the speed direction error and the detection of moving objects with complex shapes are reduced by 2.20% and 2° , respectively. The detection method in this paper reduces the time-consumption of each frame in tracking and detecting obstacles by 25,000 us and 30,000 us, respectively. The average interruption probability in a complex electromagnetic environment is lower than that obtained by the other two detection methods. The main reason for the better detection performance of this method is that virtual reality technology is used to detect road obstacles. Virtual reality technology can restore the real scene to the greatest extent, there by improving the accuracy of obstacle detection. At the same time, the ranging model used in this detection method transforms the three-dimensional Eulerian space image into a two-dimensional Eulerian space image, and calculates the data in real space from the image data, so it has high precision distance detection results.

5. CONCLUSIONS

This paper presents a method for detecting the safe distance of an unmanned vehicle based on virtual reality, which can simulate an unmanned vehicle on a computer. Various virtual simulation methods are used for different models in the scenario, and good immersion and interaction are achieved given the limited image and computing capacity of the computer. Based on the simulation results of the virtual reality experiments, more information and knowledge are extracted, and the information regarding safe distance of an unmanned vehicle is obtained by using the obstacle detection and flip perspective distance calculation model combined with threshold segmentation and decision tree. Experiments show that this method can simulate various environments and achieve accurate and efficient detection of obstacles and safe distance in these environments.

Acknowledgement

The study was supported by the National Natural Science Foundation of China — The mechanism of FDM and the coupling control of structure and performance of dual gradient bone implants (Grant No. 51705094).

REFERENCES

1. Sang, Y., Zhu, Y., & Zhao, H. (2016). Study on an Interactive Truck Crane Simulation Platform Based on Virtual Reality

Technology. *International Journal of Distance Education Technologies*, 14(2), 64–78.

2. Dahmani, H., Chadli, M., & Rabhi, A. (2015). Vehicle dynamics and road curvature estimation for lane departure warning system using robust fuzzy observers: experimental validation. *Vehicle System Dynamics*, 53(8), 1135–1149.
3. Wu, C., Hu, B., & Zhao, M. (2017). Prediction method for spatial distribution of corn borer based on unmanned aerial vehicle images and semivariance function. *Nongye-GongchengXuebao/transactions of the Chinese Society of Agricultural Engineering*, 33(9), 84–91.
4. Minaeian, S., Jian, L., & Son, Y.J. (2017). Vision-Based Target Detection and Localization via a Team of Cooperative UAV and UGVs. *IEEE Transactions on Systems Man & Cybernetics Systems*, 46(7), 1005–1016.
5. Xu, H., & Barbic, J. (2017). 6-DoF Haptic Rendering using Continuous Collision Detection Between Points and Signed Distance Fields. *IEEE Trans Haptics PP*, (99), 151–161.
6. Lee, H.Y., You, L.K., & Lee, S.M. (2015). Effects of virtual reality-based training and task-oriented training on balance performance in stroke patients. *Journal of Physical Therapy Science*, 27(6), 1883–1888.
7. Parijat, P., Lockhart, T.E., & Liu, J. (2015). Effects of Perturbation-Based Slip Training Using a Virtual Reality Environment on Slip-induced Falls. *Annals of Biomedical Engineering*, 43(4), 958–967.
8. Aravind, G., Darekar, A., & Fung, J. (2015). Virtual Reality-Based Navigation Task to Reveal Obstacle Avoidance Performance in Individuals with Visuospatial Neglect. *IEEE Transactions on Neural Systems & Rehabilitation Engineering*, 23(2), 179–188.
9. Zhong, D., Chao, L.I., & Sun, R. (2015). Scene simulation of levee-breach flood routing for high embankment canals in long-distance water diversion project. *Journal of Hydroelectric Engineering*, 34(1), 99–106.
10. Ns, V.D.B., Engelen, T., & Brouwer, O.R. (2016). A pilot study of SPECT/CT-based mixed-reality navigation towards the sentinel node in patients with melanoma or Merkel cell carcinoma of a lower extremity. *Nuclear Medicine Communications*, 37(8), 812–817.
11. Hu, X., Xu, X., & Xiao, Y. (2018). SINet: A Scale-Insensitive Convolutional Neural Network for Fast Vehicle Detection. *IEEE Transactions on Intelligent Transportation Systems PP*, (99), 1–10.
12. Zhang, J., Langbehn, E., & Krupke, D. (2018). Detection Thresholds for Rotation and Translation Gains in 360degree Video-Based Telepresence Systems. *IEEE Transactions on Visualization & Computer Graphics*, 24(4), 1671.
13. Ziraknejad, N., Lawrence, P.D., & Romill, D.P. (2015). Vehicle Occupant Head Position Quantification Using an Array of Capacitive Proximity Sensors. *IEEE Transactions on Vehicular Technology*, 64(6), 2274–2287.
14. Gke, F., Oluk, G., & Ahin, E. (2015). Vision-Based Detection and Distance Estimation of Micro Unmanned Aerial Vehicles. *Sensors*, 15(9), 23805–236.
15. Wan, P., Hao, B., & Zan, L. (2017). Accurate Estimation the Scanning Cycle of The Reconnaissance Radar Based on A Single Unmanned Aerial Vehicle. *IEEE Access PP*, (99), 1–1.
16. Peng, X., Chen, C., & Rao, Z. (2015). Safety Inspection and Intelligent Diagnosis of Transmission Line Based on Unmanned Helicopter of Multi Sensor Data Acquisition. *High Voltage Engineering*, 41(1), 159–166.
17. Wu, M. Zhang, F.T., & Wen, G.L. (2016). The Control Strategy Research of Unmanned Vehicles Steering-by-Wire System. *Computer Simulation*, 33(12), 163–168.

18. Guo, X.L. Bi, J.N., Zhang, Y., & Zhang X.H. (2016). Study on the Location-aware Based Mobile Node Aggregation Detection Method. *Journal of China Academy of Electronics and Information Technology*, 11(4), 425–428.
19. Wei, S.Y., Jiang, J.C., Zhang, W.G., & Cheng, L. (2017). Optimal Control for Efficiency of On-board Hybrid Energy Storage System in Tramway. *Journal of Power Supply*, 15(2), 77–84.
20. Wang, D., Liu, W., Li, Q.Z., & Li, K.P. (2016). Development and application of simulation system for modern tram operation. *Chinese Journal of Power Sources*, 40(10), 2040–2043.
21. Wang, J.K. (2015). Innovation of physical education teaching based on Virtual Reality Technology. *Automation & Instrumentation*, (5), 118–120.
22. Liu, L., Li, G.L., Xu, Y.B., Zhang, T., & Lv, S. (2017). Heterogeneous Parallel String Matching Algorithm Based on Mobile Platform. *Journal of Jilin University (Science Edition)*, 55(55), 88.

